

Mechanical properties and strengthening mechanisms in laser beam welds of pure titanium

H. Liu^{*1}, K. Nakata¹, N. Yamamoto² and J. Liao²

The mechanical properties and strengthening mechanisms in laser beam welds of pure titanium were investigated. Although grain coarsening is evidently observed in the heat affected zone (HAZ) and fusion zone (FZ) compared with the base metal (BM), the tensile and hardness tests indicate that the HAZ and FZ are stronger than the BM under the welding conditions employed in the present work. The strengthening mechanism in the HAZ is ascribed to the substructure strengthening and that in the FZ is attributed to the combination of the substructure strengthening and the solute solution strengthening.

Keywords: Mechanical properties, Laser beam welding, Pure titanium, Substructure, Microelement, Strengthening mechanism

Introduction

Titanium and its alloys have been widely applied in the aerospace, chemical and medical industries owing to their high specific strength, good corrosion resistance and excellent biocompatibility.¹ Therefore, the welding and joining technology is imperative in order to apply them to various products.² In the past few years, many works have been conducted to investigate the fusion welding techniques of titanium and its alloys, such as gas tungsten arc welding, gas metal arc welding, plasma arc welding, electron beam welding and laser beam welding (LBW).^{3–9} Most have concentrated on LBW because of its small welding deformation, narrow softening zone as well as convenient operation compared with electron beam welding, mainly based on the high energy density and the fast welding speed.^{6,9–14} The mechanical properties of the fusion welded joint are frequently related to the microstructure in the weld, which are strongly influenced by both the solidification and the solid phase transformation for pure titanium.^{5,14} In addition, it is commonly accepted that the mechanical properties of pure titanium are also dependent on the microelement contents and the grain orientation due to the hexagonal close packed structure.^{5,14–17} As a result, the strengthening mechanisms in the laser beam welds of pure titanium are quite complicated. Unfortunately, the previous studies have been performed with the aim of evaluating the design optimisation of the LBW technique, and little work has been reported on strengthening mechanisms in the laser beam welds of pure titanium. In the present study, the mechanical properties in the laser beam welds

of pure titanium were measured, and the strengthening mechanisms of the welds were investigated in detail by focusing on the grain structure and orientation together with the microelement contents.

Experimental

The material used in this study is a grade 2 commercially pure titanium sheet with 4 mm thickness and has a chemical composition of Ti–0.004C–0.0023H–0.078O–0.006N–0.048Fe (wt-%). The samples were bead on plate welded by an IPG YLR-10000 fibre laser welding system with a beam diameter of 0.47 mm. The focus position during LBW was kept on the top surface of the workpiece. During welding, the laser powers ranged from 8 to 10 kW, and welding speeds from 2 to 8 m min⁻¹ were selected in this investigation. Both the top and bottom surfaces of the welds were shielded using ultrahigh purity argon gas (99.999%) with a flowrate of 25 L min⁻¹ in order to minimise the surface oxidation. After welding, the laser beam welds were cross-sectioned perpendicular to the welding direction (WD) for metallographic and mechanical analysis by a wire electrical discharge cutting machine (HSC-300, Brother Ind. Ltd). The cross-sections were mechanically polished using water abrasive papers and then electropolished at room temperature for 30 s under a potential of 25 V in a solution containing perchloric acid, *n*-butyl alcohol and methanol at a volume ratio of 1:7:10. The polished cross-sections were etched in a solution comprising of hydrofluoric acid, nitric acid and distilled water at a volume ratio of 1:1:8. The etched cross-sections were examined by a scanning electron microscope (VE-8800, Keyence Corp.). Electron backscattering diffraction was used to analyse the grain structure and orientation using a scanning electron microscope (JSM-6400, JEOL Ltd) incorporated with a TexSEM Laboratories (MSC-2200; TexSEM Laboratories Inc.). Electron backscattering diffraction maps with a step size of 3.0 μm were taken

¹Joining and Welding Research Institute, Osaka University, Ibaraki 567-0047, Japan

²Technology Development Headquarters, Kurimoto Ltd, Osaka 559-0021, Japan

*Corresponding author, email hitliuhong@163.com

perpendicular to the WD, and the average confidential index from 0.55 to 0.65 was obtained. Small grains comprising fewer pixels were removed using the grain dilation option to ensure reliability, and a 10° criterion was used to define the low angle boundaries (LABs) versus the high angle boundaries (HABs). The hardness distribution at the cross-section was measured by a hardness testing machine (AAV-500, Akashi) under a load of 0.98 N for a dwell time of 15 s with an interval of 0.1 mm. The tensile test was evaluated by means of a tensile test machine (Instron-5500R, Instron Corp.) at room temperature with a crosshead speed of 2 mm min^{-1} , and three specimens with a flat surface were made for each welding condition.

Results and discussion

Mechanical properties of laser beam welds

The relationship between the mechanical properties and the grain orientation of the base metal (BM) is given in Table 1. The RD, TD and ND are the rolling, transverse and normal directions respectively. The tensile strength and hardness of BM obviously depend on the test direction, which is associated with the grain orientation or texture distribution. The tensile strength, elongation, fracture position and photographs of the tested specimens of the laser beam welds under various welding conditions are present in Table 2. The WD was parallel to the RD when a laser power of 8 kW is adopted, while the WD was perpendicular to the RD under the condition of 10 kW laser power for the tensile test. The tensile strength and elongation of the laser beam welds are approximately identical with those of BM irrespective of the welding conditions in the present work. Moreover, as seen from Table 2, all the fractures of the welds occur at the BM, far from the heat affected

zone (HAZ) and fusion zone (FZ), implying that HAZ and FZ are stronger than BM.

The hardness distributions in the laser beam welds at the laser power of 10 kW under various welding speeds are shown in Fig. 1. The fusion lines cannot be accurately identified due to the similar microstructure formed in HAZ and FZ, and thus, they were approximately distinguished according to the location of the weld root and weld toe.⁵ From Fig. 1a–d, the location of the hardness analysis is shown in the top right corner, and the average hardness of the different zones is given in the top left corner. It should be pointed out that the WD was parallel to the RD in the samples for the hardness test and microstructural observation in this work. This is to say that both the indentation direction and the observation direction are parallel to the RD. The average hardness value of the BM is $\sim 132 \text{ HV}$, quite consistent with the result shown in Table 1. Additionally, the weld width gradually becomes narrower with the increase in welding speed due to the decrease in welding heat input. The average hardness in the HAZ is almost the same under various welding speeds, but the average hardness in the FZ seems to be low at slow welding speed (compared with the fast welding speeds) because of the coarse microstructures formed at the comparatively slower cooling rate. Although an obvious scatter is detected in the HAZ and FZ as well as the BM, the average hardness in the HAZ and FZ is clearly higher than that in the BM. It can also be seen from Fig. 1 that the scatter extent of hardness in HAZ and FZ is larger than that in the BM. This phenomenon may be explained according to the textures in these regions and will be discussed in the following section.

Grain structure and orientation in laser beam welds

In order to investigate the relationship between the hardness and the grain orientation, several coarse grains with different orientations were chosen from the grain boundary map in the FZ at 10 kW laser power and 2 m min^{-1} welding speed (as shown in Fig. 2, where the indentation marks within the grain C are displayed in the top left corner). The HABs (solid black line) are the α grain boundaries, while the LABs (solid grey line) depict the substructures within the α grains. It was found that the selected grains show similar grain size and have no distinct substructures. The relationships between the

Table 1 Relationship between mechanical properties and grain orientation of BM


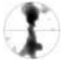
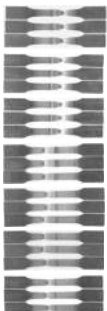
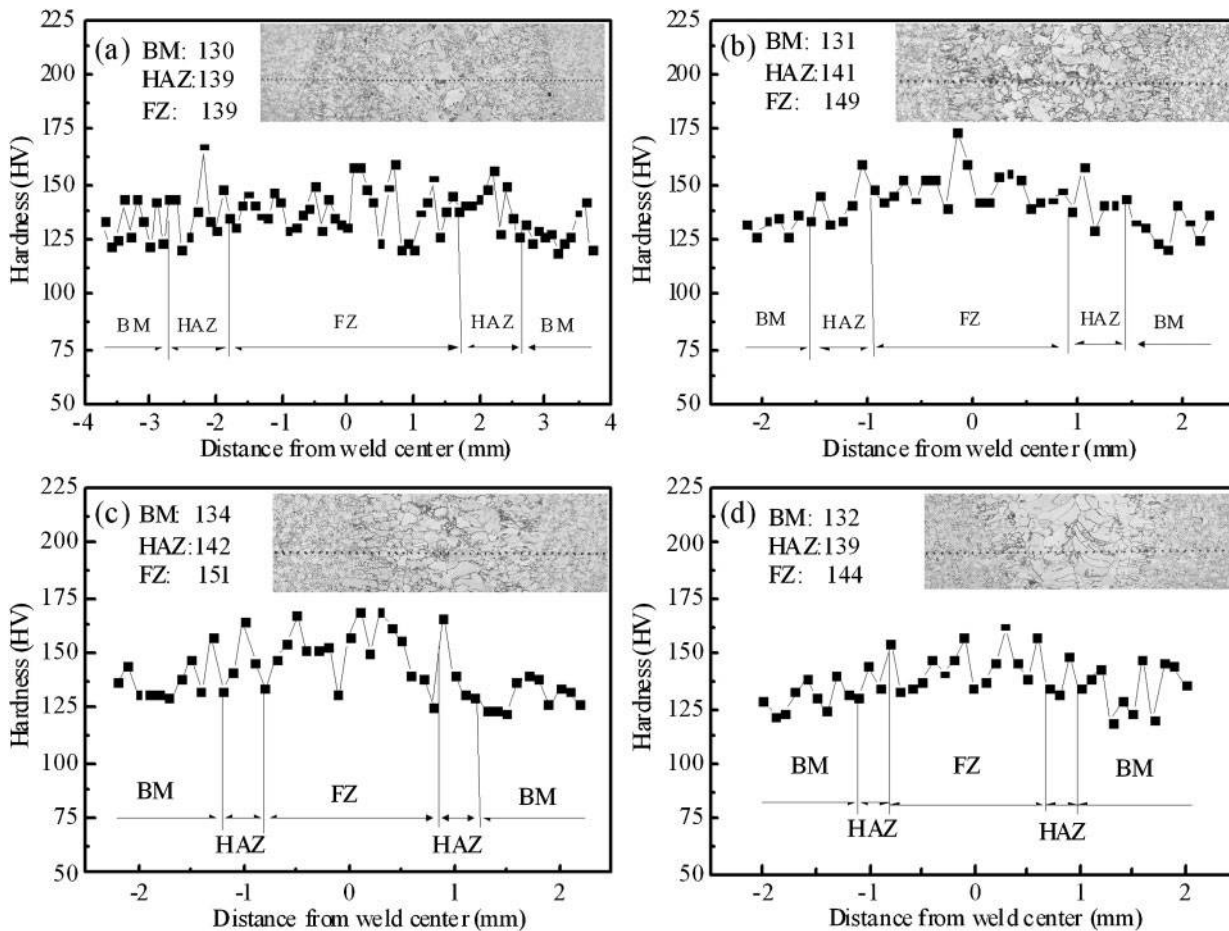
Test direction	Tensile strength/MPa	Elongation/%	Hardness/HV	(0002) pole figure
RD	386	43	132	
TD	399	37	139	

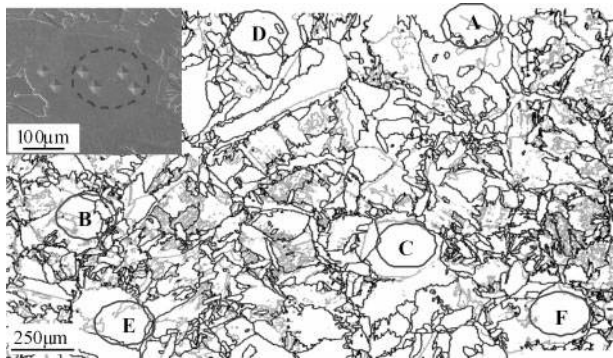
Table 2 Tensile strength, elongation, fracture position and photographs of tested specimens of laser beam welds under various welding conditions

Laser power/kW	Welding speed/ m min^{-1}	Tensile strength/MPa	Elongation/%	Fracture position	Photographs of tested specimens
8	2	393	37	BM	
	4	398	37	BM	
	6	393	37	BM	
10	2	374	45	BM	
	4	383	44	BM	
	6	372	45	BM	
	8	381	44	BM	



a 2 m min⁻¹; b 4 m min⁻¹; c 6 m min⁻¹; d 8 m min⁻¹

1 Hardness distributions in laser beam welds at laser power of 10 kW under various welding speeds



2 Grain boundary map and analysed grains of hardness test with different orientations in FZ at 10 kW laser power and 2 m min⁻¹ welding speed

hardness and the grain orientation of the analysed grains are detailed in Table 3. The relatively high hardness was detected when indenting into the basal plane, whereas the low hardness was found when indenting into the prismatic plane. Thus, the significant scatter in the

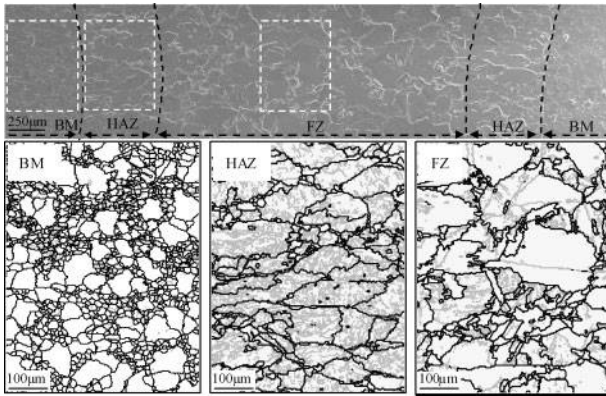
hardness distribution can be ascribed to the crystallographic anisotropy, which is nearly related to the hexagonal close packed structure of pure titanium.^{5,16,17}

The grain boundary maps of the various regions in the weld at 10 kW laser power and 4 m min⁻¹ welding speed are shown in Fig. 3 as well as a low magnification overview. Similarly, the LABs and HABs are indicated by solid grey and solid black lines respectively. As seen from the grain boundary maps in Fig. 3, the plentiful HABs and the sporadic LABs are present in the BM because of the recrystallised structure of the BM. The microstructure of the BM is a mix structure with fine and coarse grains, and the coarse grains indicate the occurrence of grain growth during the manufacturing process of pure titanium sheet. In contrast, the LABs in the HAZ and FZ are remarkably abundant, although the grain sizes in these regions are larger than that in the BM. The LABs, i.e. the substructure boundaries, are important to the strength of the welds, as discussed later.

The lengths of LABs and HABs are given in Table 4, together with the grain size, hardness, (0002) pole figure and rotated (0002) pole figure of various regions in the

Table 3 Relationships between hardness and grain orientation of analysed grains shown in Fig. 2

Zone	A	B	C	D	E	F
Hardness/(HV)	169.1 ± 6.3	151.9 ± 6.8	139.2 ± 3.1	135.7 ± 7.3	132.2 ± 6.6	118.6 ± 5.5
Orientation						



3 Low magnification overview and grain boundary maps of various regions in weld at 10 kW laser power and 4 m min⁻¹ welding speed

weld. The rotated pole figures were acquired by rotating the real pole figures 90° around the ND in order to understand the textures in these regions more clearly. An evident concentration of grain orientation with the basal plane is close to the centre part of the rotated pole figure in the BM. However, the grain orientation with the basal plane is not found to concentrate near the centre part of both the real pole figures and the rotated pole figures in the HAZ and FZ. This is different from the result observed in the friction stir weld of pure titanium.^{18,19} The texture in the BM may explain why the scatter extent of hardness in the BM is smaller than that in the HAZ and FZ. It can also be seen from Table 4 that the length of the LABs markedly increases in the HAZ and FZ, and the increased length of the LABs indicated that a large number of substructures are formed in the HAZ and FZ. The formation of substructure is mainly attributed to two aspects: the adjacent α variants inherited from one β grain may represent the close orientation due to the non-equilibrium transformation caused by fast cooling rate,²⁰ and the neighbouring α variants transformed from different β grains possibly show the same orientation because of the close orientation between the two β grains.²¹

Strengthening mechanisms in laser beam welds

As shown in Table 4, the mean grain size in the BM is $\sim 22 \mu\text{m}$, while the grain sizes in the HAZ and FZ are ~ 43 and $52 \mu\text{m}$ respectively (i.e. grain coarsening has occurred in the weld). The coarse grains usually result in a decrease in hardness and/or strength according to the Hall–Petch relation described by the following equation

$$\sigma_{\text{grain}} = \sigma_o + k_o d_{\text{grain}}^{-1/2} \quad (1)$$

Table 4 Grain size, hardness, lengths of LABs and HABs, (0002) pole figure and rotated (0002) pole figure of various regions in weld shown in Fig. 3

Region	Grain size/ μm	Hardness/HV	Length of LABs/cm	Length of HABs/cm	(0002) pole figure	Rotated (0002) pole figure
BM	22	131	0.72	4.75		
HAZ	43	141	3.42	2.32		
FZ	52	149	1.50	2.16		

where σ_{grain} is the yield stress, σ_o is the resistance to dislocation movement, k_o is the hardening contribution from the grain boundary and d_{grain} is the grain diameter.

However, the results of the hardness test shown in Table 4 cannot be explained according to the grain size, suggesting that other factors cause the strengthening of the HAZ and FZ. In fact, the increment of yield stress resulting from substructure strengthening $\Delta\sigma_{\text{substructure}}$ should be taken into account considering the existence of abundant substructures in the HAZ and FZ dissimilar with the BM. The substructure strengthening is associated with the fact that the substructure boundaries (LABs) act as a barrier to dislocation motion.^{22–24} Thus, the total yield stress in the HAZ σ_{HAZ} can be described as follows

$$\sigma_{\text{HAZ}} = \sigma_{\text{grain}} + \Delta\sigma_{\text{substructure}} \quad (2)$$

Although the grain size clearly increases in the HAZ compared with the BM, the increment of yield stress produced by substructure strengthening may lead to the final increase in total yield stress in the HAZ.

However, the active titanium element will inevitably absorb a small quantity of other elements from the surrounding environment during welding, although welds with silvery white surfaces were obtained after welding. It is well known that the strength of pure titanium depends on the microelement contents, especially on the N and O elements. The microelement contents in the weld under the condition of 10 kW laser power and 4 m min⁻¹ welding speed are shown in Table 5. The microelement contents in the FZ are actually higher than those in the BM, and the increment of yield stress generated by solute solution strengthening $\Delta\sigma_{\text{solute}}$ should also be taken into account in the FZ. The solute solution strengthening is mainly due to the fact that the solute atoms can impede dislocation motion by the interacting between the solute atoms and the dislocations.^{24,25} Therefore, the total yield stress in the FZ σ_{FZ} can be put in the form as follows

Table 5 Microelement contents in weld at 10 kW laser power and 4 m min⁻¹ welding speed

Region	Microelement contents/ppm			
	C	H	O	N
BM	37	10	601	25
FZ	41	11	651	29
Method	C: combustion infrared absorption method; H, N: inert gas fusion thermal conductivity method; O: inert gas fusion infrared absorption method.			

$$\sigma_{FZ} = \sigma_{\text{grain}} + \Delta\sigma_{\text{substructure}} + \Delta\sigma_{\text{solute}} \quad (3)$$

Although the coarsest grain is found in the FZ, the substructure strengthening and the solute solution strengthening probably result in the highest yield stress in the FZ compared with the BM and HAZ.

Conclusions

The LBW of pure titanium was carried out, and the mechanical properties and strengthening mechanisms in the welds were investigated. The tensile strengths and elongations of the laser beam welds show the same values as those of BM under the welding conditions employed in the present work, and all the fracture of the tensile specimens occurred at the BM, implying that the HAZ and FZ are stronger than the BM. Although a significant scatter is found in the hardness distribution, the average hardness in the HAZ and FZ is higher than that in the BM, which is accordant with the result of the tensile test. The welding heat input evidently leads to grain coarsening in the HAZ and FZ, and the coarse grains usually result in the decrease in hardness. However, the opposite results are found in the HAZ and FZ. The strengthening mechanism in the HAZ is due to substructure strengthening while that in the FZ is attributed to the combination of substructure strengthening and solute solution strengthening.

References

1. C. Leyens and M. Peters: 'Titanium and titanium alloys: fundamentals and applications'; 2003, Weinheim, Wiley-VCH.
2. W. A. Baeslack III, J. R. Davis and C. E. Cross: 'Selection and weldability of conventional titanium alloys', in 'ASM handbook', Vol. 6, 'Welding brazing and soldering', 507–523; 1993, Materials Park, OH, ASM International.
3. S. Sundaresan, G. D. Janaki Ram and G. Madhusudhan Reddy: 'Microstructural refinement of weld fusion zones in α - β titanium alloys using pulsed current welding', *Mater. Sci. Eng. A*, 1999, **A262**, 88–100.
4. L. Liu, X. Du, M. Zhu and G. Chen: 'Research on the microstructure and properties of weld repairs in TA15 titanium alloy', *Mater. Sci. Eng. A*, 2007, **A445–A446**, 691–696.
5. S. Lathabai, B. L. Jarvis and K. J. Barton: 'Comparison of keyhole and conventional gas tungsten arc welds in commercially pure titanium', *Mater. Sci. Eng. A*, 2001, **A299**, 81–93.
6. M. Roggensack, M. H. Walter and K. W. Böning: 'Studies on laser- and plasma-welded titanium', *Dent. Mater.*, 1993, **9**, 104–107.
7. T. Mohandas, D. Banerjee and V. V. Kutumba Rao: 'Fusion zone microstructure and porosity in electron beam welds of an α + β titanium alloy', *Metall. Mater. Trans. A*, 1999, **30A**, 789–798.
8. A. B. Short: 'Gas tungsten arc welding of α + β titanium alloys: a review', *Mater. Sci. Technol.*, 2009, **25**, 309–324.
9. Q. Yunlian, D. Ju, H. Quan and Z. Liying: 'Electron beam welding, laser beam welding and gas tungsten arc welding of titanium sheet', *Mater. Sci. Eng. A*, 2000, **A280**, 177–181.
10. P. E. Denney and E. A. Metzbowser: 'Laser beam welding of titanium', *Weld. J.*, 1989, **68**, 342s–346s.
11. F. Caiazzo, F. Curcio, G. Daurelio and F. M. C. Minutolo: 'Ti6Al4V sheets lap and butt joints carried out by CO₂ laser: mechanical and morphological characterization', *J. Mater. Process. Technol.*, 2004, **149**, 546–552.
12. S. H. Wang, M. D. Wei and L. W. Tsay: 'Tensile properties of LBW welds in Ti–6Al–4V alloy at evaluated temperatures below 450°C', *Mater. Lett.*, 2003, **57**, 1815–1823.
13. H. Du, L. Hu, J. Liu and X. Hu: 'A study on the metal flow in full penetration laser beam welding for titanium alloy', *Comput. Mater. Sci.*, 2004, **29**, 419–427.
14. C. Li, K. Muneharua, S. Takao and H. Kouji: 'Fiber laser-GMA hybrid welding of commercially pure titanium', *Mater. Des.*, 2009, **30**, 109–114.
15. X. Li, J. Xie and Y. Zhou: 'Effects of oxygen contamination in the argon shielding gas in laser welding of commercially pure titanium thin sheet', *J. Mater. Sci.*, 2005, **40**, 3437–3443.
16. T. B. Britton, H. Liang, F. P. E. Dunne and A. J. Wilkinson: 'The effect of crystal orientation on the indentation response of commercially pure titanium: experiments and simulations', *Proc. R. Soc. A*, 2010, **466A**, 695–719.
17. E. Merson, R. Brydson and A. Brown: 'The effect of crystallographic orientation on the mechanical properties of titanium', *J. Phys. Conf. Ser.*, 2008, **126**, 012020.
18. H. Fujii, Y. Sun, H. Kato and K. Nakata: 'Investigation of welding parameter dependent microstructure and mechanical properties in friction stir welded pure Ti joints', *Mater. Sci. Eng. A*, 2010, **A527**, 3386–3391.
19. H. Liu, K. Nakata, N. Yamamoto and J. Liao: 'Grain orientation and texture evolution in pure titanium lap joint produced by friction stir welding', *Mater. Trans.*, 2010, **51**, 2063–2068.
20. S. C. Wang, M. Aindow and M. J. Starink: 'Effect of self-accommodation on α/α boundary populations in pure titanium', *Acta Mater.*, 2003, **51**, 2485–2503.
21. N. Gey and M. Humbert: 'Characterization of the variant selection occurring during the $\alpha \rightarrow \beta \rightarrow \alpha$ phase transformations of a cold rolled titanium sheet', *Acta Mater.*, 2002, **50**, 277–287.
22. A. W. Thompson: 'Substructure strengthening mechanisms', *Metall. Trans. A*, 1977, **8A**, 833–842.
23. W. Zhao, W. Zhang, J. Guo, B. Wang, J. Guo and K. Lu: 'Microstructure evolution and tensile properties of pure Ti subjected to rapidly heating and quenching', *J. Mater. Sci. Technol.*, 2006, **22**, 190–194.
24. G. E. Dieter: 'Mechanical metallurgy', SI Metric edition; 1988, Singapore, McGraw-Hill.
25. M. Z. Butt and P. Feltham: 'Solid-solution hardening', *J. Mater. Sci.*, 1993, **28**, 2557–2576.